Revue des Composites et des Matériaux Avancés-Journal of Composite and Advanced Materials
Vol. 30, No. 5-6, December, 2020, pp. 195-202
Journal homepage: http://iieta.org/journals/rcma

Wear Performance of Value-Addition Epoxy/Breadfruit Seed Shell Ash Particles and Functionalized Momordica Angustisepala Fiber Hybrid Composites

Vincent C. Ezechukwu[1*], Chukwuemeka C. Nwobi-Okoye[1], Philip N. Atanmo[1], Victor S. Aigbodion[2,3]

[1] Department of Mechanical Engineering, Chukwuemeka Odumegwu Ojukwu University, Uli 431124, Anambra State, Nigeria
[2] Department of Metallurgical& Materials Engineering, University of Nigeria Nsukka, Private Bag 0004, Nsukka Enugu State, Nigeria
[3] Faculty of Engineering and Built Environment, University of Johannesburg, P. O. Box 534 Auckland Park, South Africa

Corresponding Author Email: vc.ezechukwu@coou.edu.ng

https://doi.org/10.18280/rcma.305-601

Received: 13 April 2020
Accepted: 20 November 2020

Keywords:
Momordica angustisepala fiber, breadfruit seed shell, microstructure and wear

ABSTRACT

The numerical approach for the study of wear performance of breadfruit seed shell ash particles (BFSAp) and Sodium hydroxide (OH)/silane (APS)functionalized Momordica angustisepala fiber (MAf)/epoxy hybrid composites were investigated. The MAf fibers were treated with an OH-APS solution. Hardness values, wear rate and wear mechanism of the samples were determined. A 65.82% improvement in wear resistance was obtained at the load of 30N of 30wt%MAf-20wt%BFSAp composite. The wear rate and wear damage followed in this order: epoxy(matrix)<epoxy/30wt%MAf-20wt%BFSAp<epoxy/OH-APS treated 30wt%MAf-20wt%BFSAp composites. The wear mechanism observed in this work is a combination of abrasive and adhesive wear. High wear resistance was obtained in epoxy/OH-APS treated 30wt%MAf-20wt%BFSAp composites.

1. INTRODUCTION

The hybrid composites are been developed in recent times to overcome the limitation of single reinforcement composites and polymer in the area of high hardness values, wear resistance, thermal and fire resistance [1]. These limitations make polymer materials not suitable in the manufacturing of bolted flange, automobiles component, pipeline, and marine equipment, etc. [2]. Among the recent work on hybrid composites is the combination of particular and fibers in the production of composites materials. The hybrid composites have several advantages such as high tensile, flexural strength, elastic, impact energy, thermal stability, abrasion and wear resistance [3].

Research has been made in recent years to developed multifunctional composites. Gill and Sidhu [4] reported on the wear resistance of epoxy hybrid composites using B4C and WS2 as reinforcing materials. The wt% of B4C and WS2, sliding speed and applied load were varied. The applied load has a higher effect on the wear behavior of the developed composites. Mahesha et al. [5] studied the erosive wear of epoxy hybrid composites using Basalt and Nano clay/TiO_2 as a reinforcing material. The erosion wears increase with an increased in temperature and velocity of impact. Higher erosion resistance was obtained with Nano TiO_2 addition. Suresha et al. [6] determined the tribological and mechanical properties of 55wt% carbon fiber and 2.5 and 5wt% silicon carbide whiskers epoxy hybrid composites. The mechanical properties of the carbon fiber-epoxy composites were enhanced. The combination of 55wt% carbon fiber and 2.5 and 5wt% silicon carbide whiskers epoxy has excellent wear resistance. Selmy et al. [7] reported on the pin on disc wear test of epoxy hybrid composites with glass and polyamide as reinforcing materials. The stacking sequence, hybridization of the reinforcement and reinforcement percentage was used to determine the wear rate under wet and dry conditions. The reinforcement percentage has a higher impact on the wear rate, followed by the stacking sequence. Sudheer et al. [8] determined the wear and mechanical properties of epoxy hybrid composites with graphite, glass and PTW as reinforcing materials. They observed improvement in the wear behavior of the hybrid composites.

From the literature above, it was observed that there little or no information on the wear properties of breadfruit shell ash particles and Momordica angustisepala fiber (MAf) reinforced epoxy composites. Hence, the aim of this work is to study wear behavior of breadfruit shell ash particles and functionalized Momordica angustisepala fiber (MAf) reinforced epoxy composites.

Momordica angustisepala fiber (MAf) is one of the promising natural fibers for the production of polymer composites [9]. The fibers can be obtained in many Africa countries such as Nigeria, Cameroon, Ghana, Benin and Cote Divoire etc. [10]. The fibers are obtained from MA stem by pounding and washing of the fibers to remove impurities [11]. The MA fibers are used in Africa as a local sponge for bathing [11]. Achigan-Dako [12] used MA as local medicine in Nigeria, Atuanya et al. [10] characterized MAf for possible use for polymer composites production. They observed tensile strength of 35-57.93MPa and tensile modulus 2-4.4GPa.

Breadfruit is a food plant planted in many Africa countries such as Nigeria, Angola, Togo, Ghana, Sudan, Senegal, Sierra

Leone, and Cameroon, etc. [13]. The breadfruit seed is cultivated and the shell is removed from the seed. The seed is eaten as food while the shell is dumped to the ground or open burning causing environmental pollution [14]. Atuanya et al. [14] developed Al-Si-Fe alloy composites reinforced with breadfruit seed shell ash particles. Breadfruit seed shell ash particles of particle size of 500nm were used in the production of the composites. They concluded that the tensile strength and hardness values improved as the weight % breadfruit seed shell ash particles is increased in the formulation with slightly decreased in impact energy. Atuanya et al. [15] developed composites materials using low-density polyethylene and breadfruit seed shell ash particles. The breadfruit seed shell ash particles were varied from 5-25wt% with 5wt% interval. They observed good distribution of breadfruit seed shell ash particles in the polymer and better mechanical properties.

2. MATERIALS AND METHOD

The MA fibers were cleaned with acetone for 48hrs and oven-dried at 75℃ for 5hrs [16]. The cleaned fibers bundle was kept in a glass container. The cleaned MA fibers were soaked in 80ml sodium hydroxide (OH) solution and were heated to a temperature of 105℃ for 3hrs after then the fibers were washed with 5%HCl solutions and dried in the oven at 75℃ to obtain hydroxylated fibers [17]. The silane fictionalization was done by preparing 2ml of Amino propyltriethoxy silane (APS) in 100ml ethanol at a temperature of 150℃ and time of 2 hours [18] (see Figure 1). This chemical treatment was done to enhance the interfacial bonding between the polymer and reinforcement used.

Figure 1. Chemical treatment of MA fibers

Before the breadfruit seed shell was used in the production of the composites. The breadfruit seed shell was sun-dried for three days and pulverized into a fine powder. The pulverized powder was packed in a crucible made of graphite and placed in a muffle electric furnace. The furnace was heated to a temperature of 1000℃ and hold for 5hours. The particle size of the breadfruit seed shell powder sample after heating was done and a size of 63µm was used in the research [19]. X-ray fluorescence (XRF) model X-MET 8000 was used to determine the composition of the BFSAp.

A white Epoxy resin LY556 (HERENBA BRAND) and Hardener (HY951) was used in the production of the composites. The average diameter (d) of 0.105mm and continues length (L) of 20cm were used in the production of the hybrid composite. The hand-laying method was used in the production of the hybrid composites of epoxy/30wt%MAf-20wt%BFSAp and epoxy/OH-APS treated 30wt%MAf-20wt%BFSAp. The samples were cured at a temperature of 150℃ and 4hours [16]. The produced samples are shown in Figure 2.

Figure 2. Photograph of produced samples

Leeb portable hardness tester was used to determine the hardness values of the samples using ASTM A1038-19. Equinox 55 FTIR model Fourier infrared was used to determine the functional group of the composites. Siemens D-5000 model X-ray diffractometer was used to determine the crystallinity index of the composites. SEM model JEOL JSM840A was used to determine the microstructure of the composites. ASTM G 99-5 standard was used to determine the dry wear behavior of the composites using the TRN tribometer machine. The initial weight of the specimen was measured using an electronic weighing machine with an accuracy of 0.01gm. The wear and coefficient of friction were determined and the final mass of the specimen was noted. The wear rate of the samples was calculated using Eq. (1) [8].

$$WR=\Delta W/\text{ḍ} \times D \quad (1)$$

where, WR=wear rate (mm^3/m), ḍ=Density of the composite (g/cm^3), ΔW=Weight loss (g) and D=Sliding distance (m), the results for the coefficient of friction were recorded as the mean value for friction as generated by the machine.

3. RESULTS AND DISCUSSION

3.1 Composition of the fibres

The treated and untreated MA fibers were immersed in the toluene/ethanol solution (2:1%v/v) before there composition was determined [16]. The results obtained are displayed in Figure 3. It was clear that OH-APS treatment of MAf decreases the amount of wax, hemicelluloses and impurities. The decreased in wax, hemicelluloses and impurities obtained could be attributed to the fact that the treatment of the fibers with OH-APS activates the O-H and hydrolyzable alkoxy group to formed silanols. A similar observation was obtained by Fath et al. in the work [20, 21].

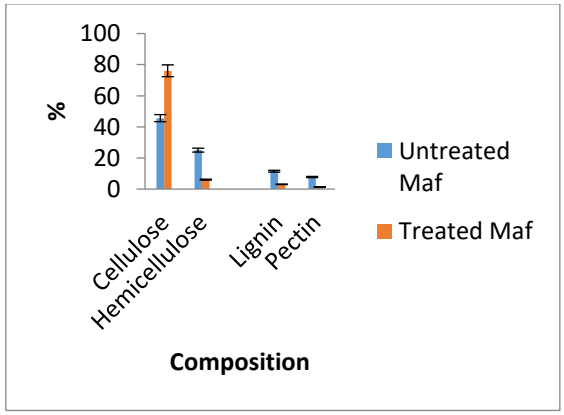

Figure 3. Composition of the fiber

Table 1. Composition of BFSAp

Element	SiO_2	P_2O_5	SO_3	K_2O	CaO	TiO_2	MnO	Fe_2O_3	BaO	EuO_3
%	8.5	6.01	2.0	30.5	30.6	0.25	0.09	17.8	0.3	3.7

3.2 Composition of the BFSAp

X-ray fluorescence (XRF) analysis was used to determine the chemical composition of the BFSAp. The result of the XRF is displayed in Table 1. From Table 1, it was seen clearly that the major components of BFSAp are: K_2O (30.5%), CaO (30.6%), Fe_2O_3 (17.8%), SiO_2 (8.5%) and P_2O_5 (6.01%). The result obtained is in par with the BFSAp earlier analyzed by Atuanya et al. [13].

3.3 Microstructure of the MAf and BFSAp

Figures 4-5 displayed the SEM/EDS of the treated and untreated MAf. The SEM images show that fibers are longitudinal and straight in shapes. It was seen clearly in Figure 5 that the SEM images of the treated MAf were cleaned and straight fibers without grooves. The chemical treatments help to remove the waxy epidermal tissue, hemicelluloses in the MAf. This is in par with the work of the refs. [21, 22]. In the EDS of Figure 5, the presence of Si in the OH-ASP treated MAf shows that the hydrolyzable alkoxy group formed silanols [22].

Figure 6 displayed the SEM/EDS of the BFSAp. The microstructure of the BFSAp shows that the particles are round, spherical in shapes and randomly distributed. In Figure 6 it was observed that the particle size varies from fine, medium and coarse. These particles help to close the interlocking chains of the polymer, and hence increase of the strength of the composites. The EDS has a high peak of K and Ca, this is in par with the result of the XRF discussed above that BFSAp contain a high amount of K_2O and CaO.

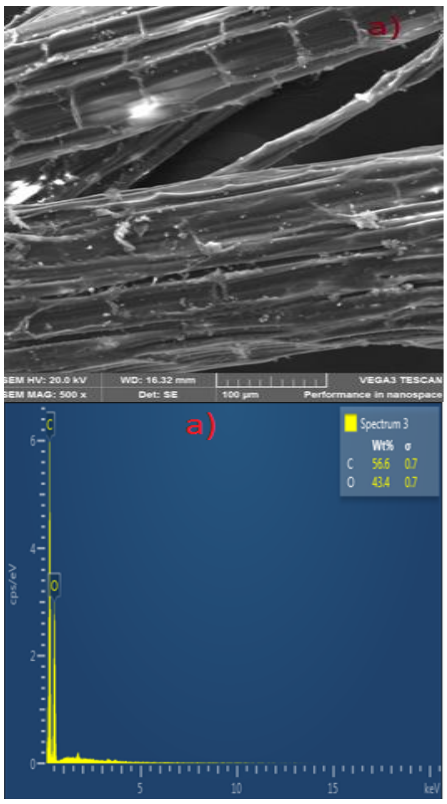

Figure 4. SEM/EDS of the untreated MA Fiber

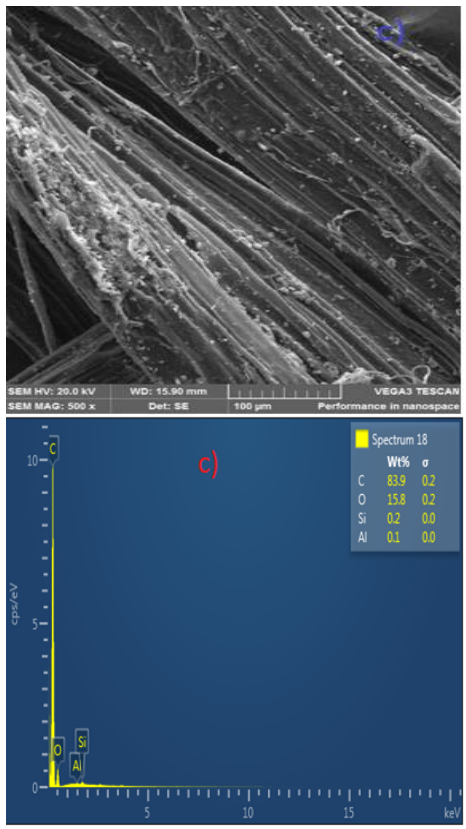

Figure 5. SEM/EDS of the treated OH-APS MA Fiber

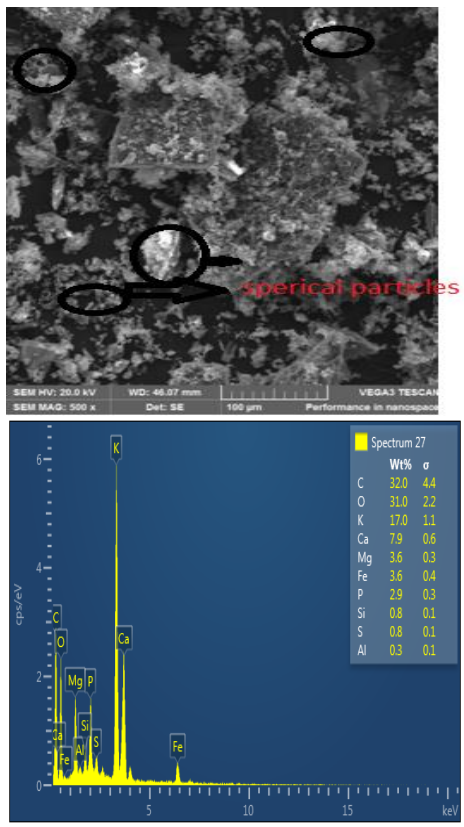

Figure 6. SEM/EDS of the BFSAp

3.4 FTIR analysis

Figure 7 and Table 2 displayed the FTIR of the epoxy, epoxy/30wt%MAf-20wt%BFSAp and epoxy/OH-APS treated 30wt%MAf-20wt%BFSAp respectively. It was observed that the FTIR curves of all the samples in question are similar with some minor peaks in the epoxy/OH-APS treated 30wt%MAf-10wt%BFSAp sample (see Figure 7). The minor difference in the FTIR is as a result of the OH-APS attack on the surface of the MAf. Stretching vibration of 3000cm^{-1} of O-H was observed in all samples. Stretching vibration of 2916 cm^{-1} is the CH_2 of the silane treated composite. The OH-APS treated composite, revealed COH scissoring vibration at 895.5cm^{-1}. The NH_2 bending in the OH-APS treated composite occurred at1634cm^{-1} Si-C group was visible in the OH-APS treated fibers at 1322cm^{-1} with an increase in the NH_2 group. An increase in the NH_2 will helps in increasing bonding between the polymer and the fibers [22].

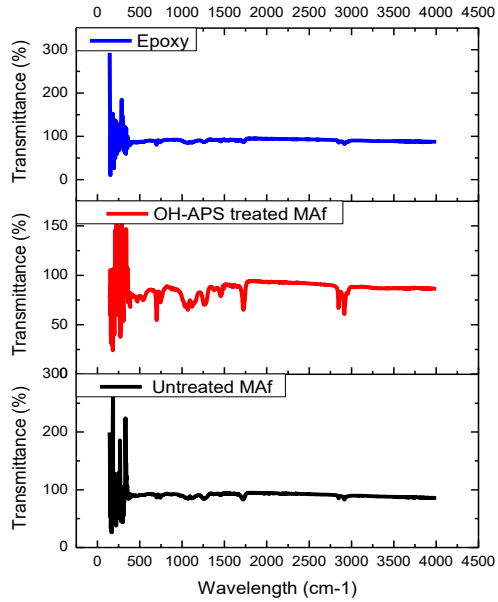

Figure 7. FTIR analysis of the composites

Table 2. FTIR analysis

Wave length(cm^{-1})	Epoxy	Untreated MAf	OH-APS treated MAf
3000	O-H	O-H	O-H
2916			CH_2
1634			Si-C
1322			NH_2
895.5			COH

3.5 Crystallinity index

The X-ray diffraction patterns of composites are given in Figure 8. The crystallinity index (CrI) of the composites were calculated according to the empirical method shown in the following Eq. (2):

$$\%CI = \frac{I_{002} - I_{am}}{I_{002}} X100 \qquad (2)$$

where, I_{002} and I_{am} are the peak intensities of crystalline and amorphous materials, respectively.

The major peaks observed for samples at 2θ diffraction angles were around 10.15 and 20.17°. The first peaks at 10.15° are the low angle reflection representing I(am) of amorphous material with the intensity counts of: 1856, 2083, 2436 for the epoxy, epoxy/30wt%MAf-20wt%BFSAp and epoxy/OH-APS treated 30wt%MAf-20wt%BFSAp respectively. While the reflection at 20.17° represented I(002) of crystalline material with intensity counts of: 2150, 3761, 6772 for the epoxy, epoxy/30wt%MAf-20wt%BFSAp and epoxy/OH-APS treated 30wt%MAf-20wt%BFSAp respectively (see Figure 8). Values of 13.67, 44.61 and 64.03% were obtained for the crystallinity index for the epoxy, epoxy/30wt%MAf-20wt%BFSAp and epoxy/OH-APS treated 30wt%MAf-20wt%BFSAp respectively. It was seen that the degree of crystallinity index of the treated composite is higher than the untreated composite and epoxy. This could be attributed to the removal of hemicellulose which results in close packing of the cellulosic chain [23]. A similar observation of an increase in the crystallinity index of composite has been reported in the literature [24].

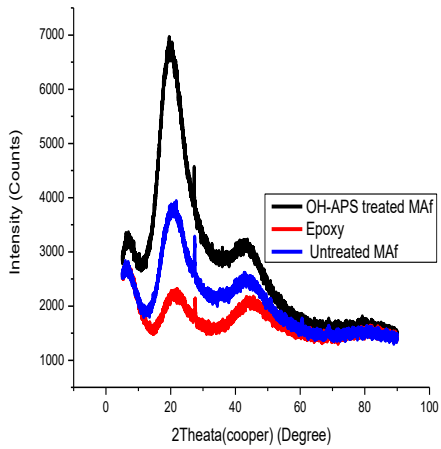

Figure 8. X-ray diffraction analysis of the composites

3.6 Hardness values

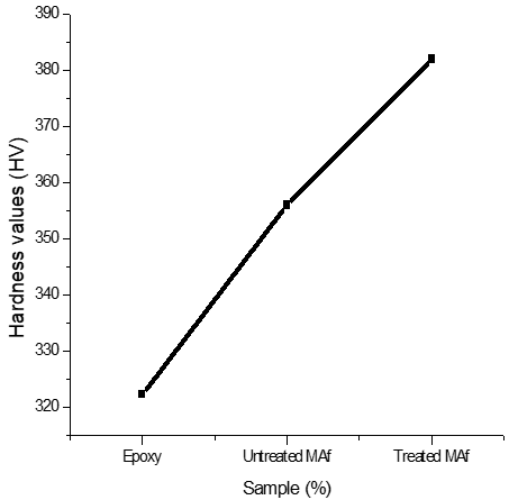

Figure 9. Variation of hardness values with sample condition

The hardness results obtained in this work are displayed in Figure 9. In Figure 9, it was observed that the hardness values of the materials under study are close. For example, hardness values of 322.33, 356.00 and 382.00 HV were obtained for the

epoxy, epoxy/30wt%MAf-20wt%BFSAp and epoxy/OH-APS treated 30wt%MAf-20wt%BFSAp composites respectively. The brittle nature of the epoxy helps to increase the hardness values of the polymer. However, increases in the hardness values of the composites could be attributed to BFSAp addition which contains a hard oxide of K_2O, CaO and Fe_2O_3. It can be concluded in this work that particles-fiber strengthening of the epoxy matrix can be achieved with the combination of MAf and BFSAp to obtained high hardness values which can be used in the production of flange bolt and automobile components [16].

3.7 Wear results

The coefficient of friction results for the various loads of 10, 20 and 30N and speed of 2.5m/s are displayed in Figure 10. It was observed that the coefficient of friction was greatly affected by the applied load, time and sample condition. The coefficient of friction linearly increased with time and load (see Figure 10). The coefficient of friction is higher as the applied load increases from 10 to 30N (see Figures 11-12). Coefficient of friction of 0.04, 0.45 and 0.072 were obtained for the epoxy at a load of: 10, 20 and 30N. Also, coefficient of friction of 0.024, 0.035, 0.038 and 0.017, 0.019 and 0.021 were obtained for: epoxy/30wt%MAf-20wt%BFSAp and epoxy/OH-APS treated 30wt%MAf-20wt%BFSAp composites respectively at the same applied load of: 10, 20 and 30N. The increases in coefficient friction with applied load could be attributed to the fact that when applied load increases, the pressure applied in the sample raise which leads to increase the friction of the materials [6, 7]. The coefficient of friction rises from epoxy, followed by epoxy/30wt%MAf-20wt%BFSAp and epoxy/OH-APS treated 30wt%MAf-20wt%BFSAp composites respectively.

Figure 13 displayed the wear rate of the samples. From Figure 13, it can be seen clearly that wear rate has a similar pattern with coefficient of friction. As the applied load increases results in reduction of wear resistance of the samples. Increases in wear rate as the applied load increases from 10N to 30N could be attributed to increase in deep of penetration of the materials and increase in shear stress at the surface which increases materials removal at the surface. When applied load increases lead to raises in the critical surface energy which led to an increase in the frictional forces and reduced the hardness values of the materials in question. Also, higher pressure on the samples with increase in the temperature of the samples may weaken the matrix-fiber-particles interphase can be obtained with higher applied load [9, 10].

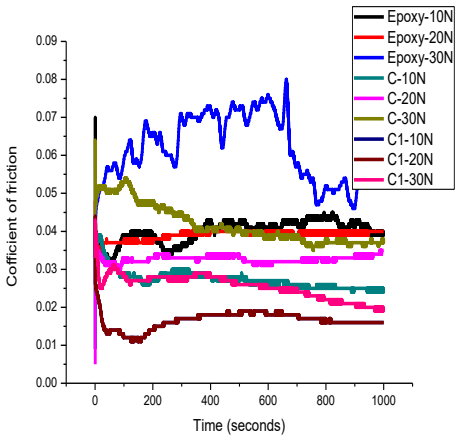

Figure 10. Variation of Coefficient of friction with time

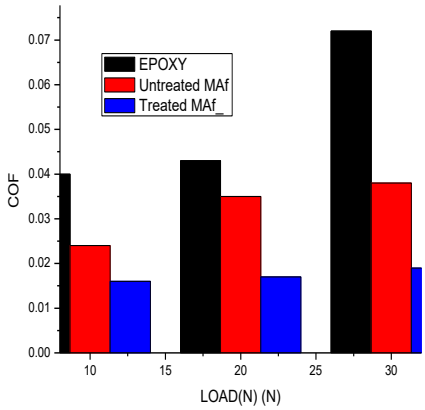

Figure 11. Variation of coefficient of friction with applied load

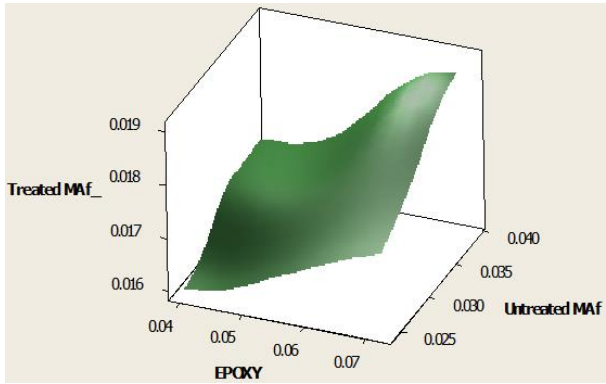

Figure 12. Variation of coefficient of friction with sample condition

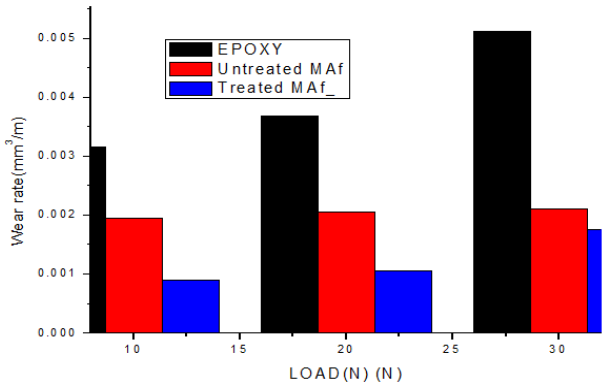

Figure 13. Variation of Wear rate with sample condition

A wear rate of 0.00315, 0.00357 and 0.00512mm^3/m were obtained for the epoxy matrix at applied load of: 10, 20 and 30N. A wear rate of 0.00195, 0.00205, 0.00211 mm^3/m and 0.000904, 0.00105 and 0.00175 mm^3/m were obtained at applied load of: 10, 20 and 30N for the epoxy/30wt%MAf-20wt%BFSAp and epoxy/OH-APS treated 30wt%MAf-20wt%BFSAp composites. A 65.82% improvement in wear resistance was obtained at a load of 30N with treated 30wt%MAf-20wt%BFSAp composites over that of the epoxy matrix. The wear rate of the samples under investigation are in the following order: epoxy (matrix)<epoxy/30wt%MAf-20wt%BFSAp<epoxy/OH-APS treated 30wt%MAf-20wt%BFSAp composites. The developed composites have a higher wear resistance.

Figure 14 shows optical images of the wear track morphology of the samples loaded with 30 N. The observed wear mechanism included abrasive and adhesive wear. Figures 14 (a-c) revealed aggressive material removal with wide wear tracks. The plowed debris was found to be sticking to the wear track; these would be considered as adhesive wear. In Figure 14, it was recorded that the wear track depth of the epoxy initially at the beginning of the wear process was 32.94µm and 29.0028 µm at the end of the wear process. A similar observation was obtained for the composites with wear track depth of: 30.90 µm to 21.24 µm and 18.55 µm to 17.27 µm for epoxy/30wt%MAf-20wt%BFSAp and epoxy treated 30wt%MAf-20wt%BFSAp. These wear track obtained for the developed composites were used to support the earlier conclusion that the composites have a high wear resistance than the epoxy. The higher wear resistance obtained for the epoxy treated 30wt%MAf-20wt%BFSAp composite could be attributed to the presence of hydrolyzable alkoxy group which formed silanols [22-24].

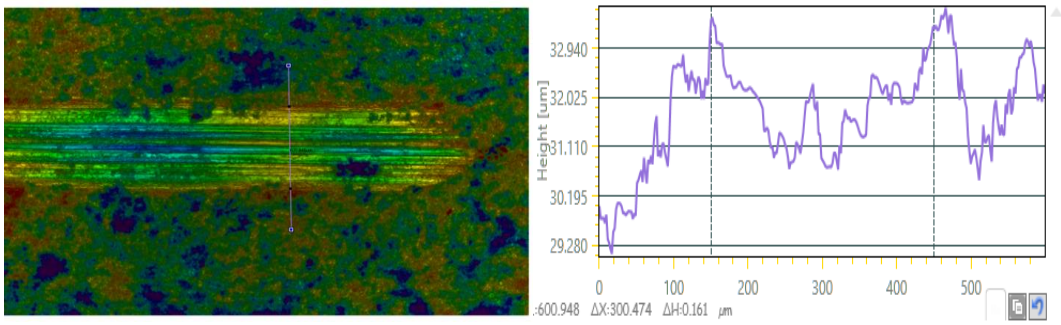

a. Wear track of the epoxy matrix at load of 30N and 2.5m/s

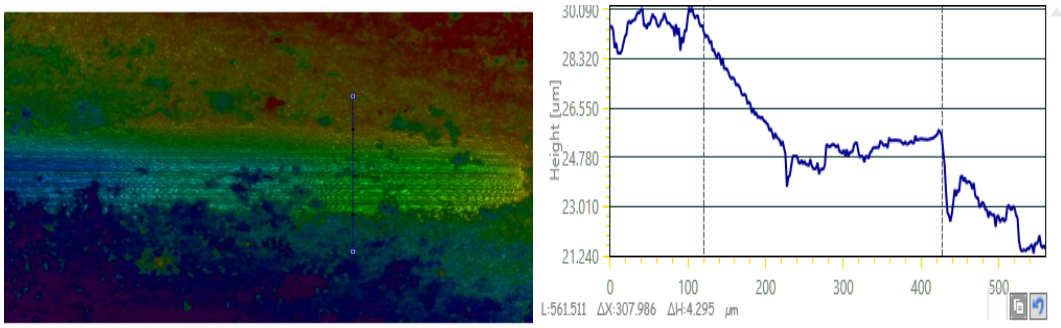

b. Wear track of the epoxy-30wt%MAf-20wt%BFSAp at load of 30N and 2.5m/s

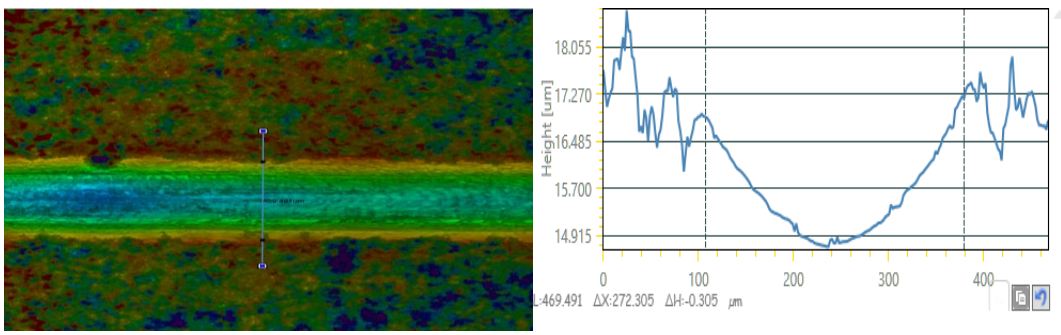

c. Wear track of the epoxy-treated 30wt%MAf-20wt%BFSAp at load of 30N and 2.5m/s

Figure 14. Wear track of the samples at applied load of 30N and 2.5m/s

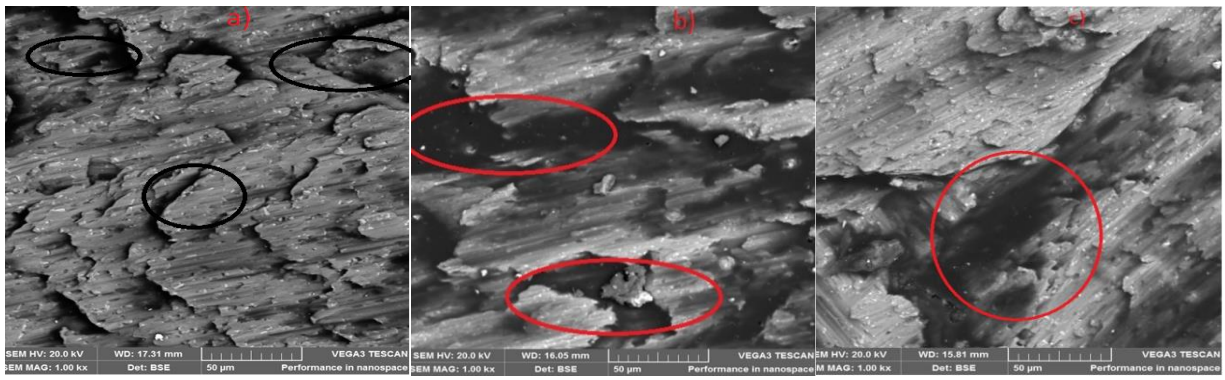

a. Wear fracture surface of the Epoxy matrix on a) Load of 10N b) Load 20N c) 30N

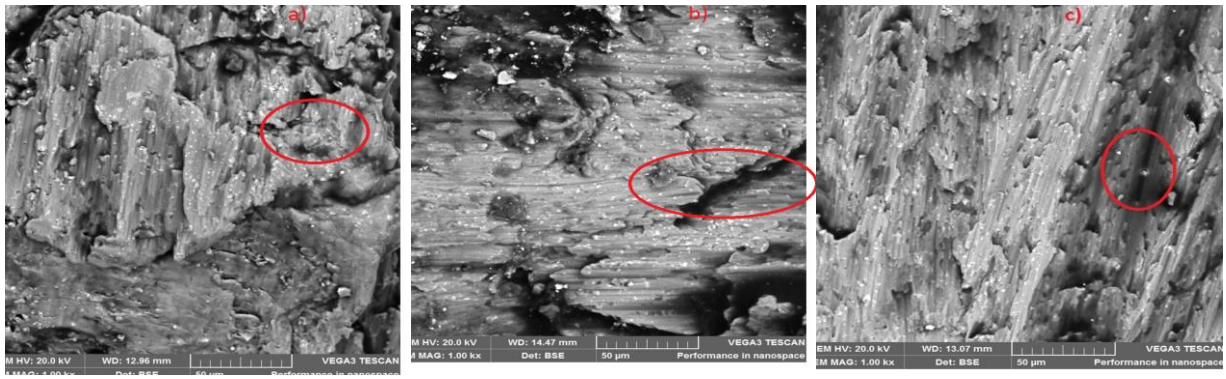

b. Wear fracture surface of the Epoxy/30wt%MAf-20wt%BFSAp on a) Load of 10N b) Load 20N c) 30N

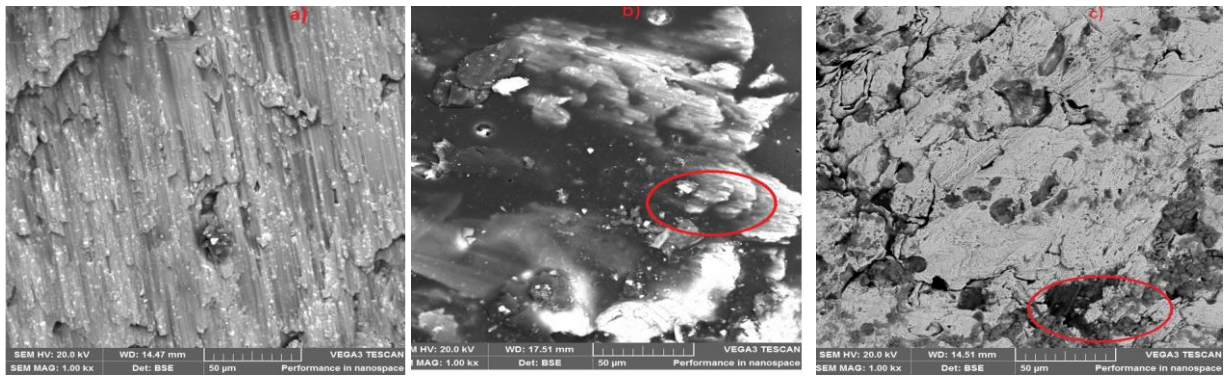

c. Wear fracture surface of the Epoxy/OH-APS 30wt%MAf-20wt%BFSAp on a) Load of 10N b) Load 20N c) 30N

Figure 15. Wear fracture surface of the samples

Figure 15 shows SEM images of the wear track morphology of the samples loaded at applied load of 10, 20 and 30N. There was a significant difference in the worn surface of the three samples under investigation. The wear damages were more pronounced in the unreinforced matrix than the composites (compared Figure 15a with Figure 15b-c). There is a strong deterioration of the wear surface as the applied load increase from 10N to 30N in both the epoxy and composites samples under investigation. Great deep of penetration was observed at the higher load of 30N (see Figure 15). The presence of wear debris, plow and adhesive wear surface was more visible in the epoxy matrix than the composites. The wear damage observed in this work followed in this order epoxy (matrix)<epoxy/30wt%MAf-20wt%BFSAp<epoxy/OH-APS treated 30wt%MAf-20wt%BFSAp composites. Crater formation, shearing of fibers and detachment of the fiber from the matrix was not observed in the composites. The wear mechanism observed in this work is a combination of abrasive and adhesive wear.

4. CONCLUSIONS

New information was obtained in the course of this work:

1. The higher crystallinity index for the functionalized OH-APS treated MAf help to improve the wear resistance of the composites.
2. The coefficient of friction was greatly affected by the applied load and time.
3. A 65.82% improvement in wear resistance was obtained at a load of 30N of treated 30wt%MAf-20wt%BFSAp composite.
4. The higher wear resistance obtained for epoxy treated 30wt%MAf-20wt%BFSAp composite was attributed to the presence of a hydrolyzable alkoxy group.
5. The presence of wear debris, plow and adhesive wear surface was more visible in the epoxy matrix than the composites.
6. The wear mechanism observed in this work is a combination of abrasive and adhesive wear.

REFERENCES

[1] Jia, C.Y., Zhang, R.Z., Yuan, C.C., Ma, Z.Y., Du, Y.Z., Liu, L., Huang, Y.D. (2020). Surface modification of Aramid fibers by amino-functionalized silane grafting to improve the interfacial property of Aramid fibers reinforced composite. Polymer Composites, 45(41): 2046-2053. https://doi.org/10.1002/pc.25519

[2] Sarker, F., Karim, N., Afroj, S., Koncherry, V., Novoselov, K.S., Potluri, P. (2018). High-performance graphene-based natural fiber composites. ACS Appl. Mater. Interfaces, 10(40): 34502−34512. https://doi.org/10.1021/acsami.8b13018

[3] Suresha, B., Guggare, S.L., Raghavendra, N.V. (2016). Effect of TiO_2 filler loading on physico-mechanical properties and abrasion of jute fabric reinforced epoxy composites. Materials Sciences and Applications, 7(9): 510-526. https://doi.org/10.4236/MSA.2016.79044

[4] Gill, C.S., Sidhu, J.S. (2016). Dry sliding wear behavior of epoxy-based composites filled with WS_2 andB_4C. International Journal of Material Sciences and Technology, 6(1): 21-32.

[5] Mahesha, C.R., Shivarudraiah, Chandra, C.R., Suprabha, R. (2015). Effect of nano TiO_2/clay on the erosive wear behavior of basalt-epoxy hybrid composites at elevated temperatures. Applied Mechanics and Materials, 813-814: 40-45. https://doi.org/10.4028/www.scientific.net/AMM.813-

814.40
[6] Suresha, B., Adappa, K., Subramani, N.K. (2018). Mechanical and tribological behaviours of epoxy hybrid composites reinforced by carbon fibers and silicon carbide whiskers. Materials Today: Proceedings, 5(8): 16658-16668. https://doi.org/10.1016/j.matpr.2018.06.027
[7] Selmy, A.I., Abd El-baky, M.A., Hegazy, D.A. (2018). Wear behavior of glass-polyamide reinforced epoxy hybrid composites. Journal of Thermoplastic Composite Materials, 33(2): 214-235. https://doi.org/10.1177/0892705718805127
[8] Sudheer, M., Hemanth, K., Raju, K., Bhat, T. (2014). Enhanced mechanical and wear performance of epoxy/glass composites with PTW/Graphite hybrid fillers. Procedia Materials Science, 6: 975-987. https://doi.org/10.1016/j.mspro.2014.07.168
[9] Shehu, A., Salami, L.B., Gbadamasi, A.A., Issa, S.B., Aliyu, M.A., Egharevba, G., Adisa, M.J., Bale, M.I., Hamid, A.A. (2019). Chemical composition from the leaf extracts of Momordica angustisepala with its antibacterial, antifungal and antioxidant activities. Nigerian Journal of Chemical Research, 24(2): 56-66.
[10] Atuanya, C.U., Ebunoha, E.O., Isaac, G.O., Aigbodion, V.S. (2012). Characterization of the thermo-mechanical behavior of Momordica angustisepala fiber intended for the manufacturing of polymer composites. Pacific Journal of Science and Technology, 14(2): 40-47.
[11] Ede, A.N., Olofinnade, O.M., Ugwu, E.I., Salau, A.O. (2018). Potentials of Momordica angustisepala fiber in enhancing strengths of normal portland cement concrete. Cogent Engineering, 5(14): 31-53. https://doi.org/10.1080/23311916.2018.1431353
[12] Achigan-Dako, E.G. (2012). Momordica angustisepala harms. In book: Plant Resources of Tropical Africa 16. Fibres, Publisher: PROTA Foundation, Wageningen, Netherlands, Editors: Martin Brink, Enoch Gbenato Achigan-Dako.
[13] Atuanya, C.U., Aigbodion, V.S., Nwigbo, S.C. (2012). Characterization of breadfruit seed hull ash for potential utilization in metal matrix composites for automotive application. People's Journal of Science & Technology, 2(1): 1-7.
[14] Atuanya, C.U., Ibhadode, A.O.A., Dagwa, I.M. (2012). Effects of breadfruit seed hull ash on the microstructures and properties of Al-Si-Fe alloy/breadfruit seed hull ash particulate composites. Results in Physics, 2: 142-149. https://doi.org/10.1016/j.rinp.2012.09.003
[15] Atuanya, C.U., Nwaigbo, S.C., Igbokwe, P.K. (2014). Effects of breadfruit seed hull ash particles on microstructures and properties of recycled low density polyethylene/breadfruit seed hull ash composites. Scientia Iranica, 21(3): 792-802.
[16] Ezechukwu, V.C. (2020). Development of Eco-friendly Polymer Composites for Bolted Flange Joint in Oil and Gas Applications using Sustainable Materials, Ph.D ongoing, Department of Mechanical Engineering, Chukwuemeka Odumegwu Ojukwu University, Anambra State Nigeria.
[17] Aigbodion, V.S., Edokpia, R.O., Asuke, F., Eke, M.N. (2018). Development of egg shell powder solution as ecofriendly reagent: for chemical treatment of natural fibers for polymer composites production. J. Mater. Environ. Sci., 9(2): 559-564. https://doi.org/10.26872/jmes.2018.9.2.61
[18] Odera, R.S., Onukwuli, O.D., Aigbodion, V.S. (2019). Effect of alkali-silane chemical treatment on the tensile properties of raffia palm fibre. Australian Journal of Multi-Disciplinary Engineering, 15(1): 91-99. https://doi.org/10.1080/14488388.2019.1648961
[19] Xie, Y.J., Hill, C.A.S., Xiao, Z.F., Militz, H., Mai, C. (2010). Silane coupling agents used for natural fiber/polymer composites: A review. Composites: Part A, 41: 806-819. https://doi.org/10.1016/j.compositesa.2010.03.005
[20] Pai, A.R., Jagtap, R.N. (2015). Surface morphology & mechanical properties of some unique natural fiber reinforced polymer composites-A Review. Journal of Materials and Environmental Science, 6(4): 902-917.
[21] Fathi, B., Foruzanmehr, M., Elkoun, S., Robert, M. (2019). Novel approach for silane treatment of flax fiber to improve the interfacial adhesion in flax/bio epoxy composites. Journal of Composite Materials, 53(16): 2229-2238. https://doi.org/10.1177%2F0021998318824643
[22] Hossain, S.M., Hasan, M., Hasan, S.M.N., Hassan, V. (2013). Effect of chemical treatment on physical, mechanical and thermal properties of ladies finger natural fiber. Advances in Materials Science and Engineering, 2013: 1-6. https://doi.org/10.1155/2013/824274
[23] Abdelmouleh, M., Boufi, S., ben Salah, A., Belgacem, M.N., Gandini, A. (2002). Interaction of silane coupling agents with cellulose. Langmuir, 18(8): 3203-3208. https://doi.org/10.1021/la011657g
[24] Asim, M., Jawaid, M., Abdan, K., Ishak, M.R. (2016). Effect of alkali and silane treatments on mechanical and fibre-matrix bond strength of kenaf and pineapple leaf fibres. Journal of Bionic Engineering, 13: 426–435. https://doi.org/10.1016/S1672-6529(16)60315-3